Principles of the Complete Voronoi Diagram Localization

Gang Lu, Mingtian Zhou, *Senior Member*, *IEEE*, Xiaoming Wang, Xiang-Yang Li, *Fellow*, *IEEE*, Xiaojun Wu, and Yumei Zhang

Abstract—This paper explores the rationale behind the Complete Voronoi Diagram (CVD) Localization, which is a computational geometry approach to the wireless network localization. Our work consists mainly of three parts. The first part focuses on the analysis of CVD's mathematical properties. We characterize CVD's central tendency as the mirror-image distribution and provide mathematical formula for its probability density function. We also provide a closed formula for the relationship between CVD's vertices, chords and faces, the average chord length, the average edge number of a CVD polygon. And the expressions for the average overall and local positioning error are also provided. Based upon these findings, we show that the convergence speed for a CVD based localization scheme is quadratic, and the optimal time and space complexities are $\Theta(n^2)$ and $\Theta(n)$, respectively. The second part proposes a novel approach, called Polling, which utilizes the concept of the Error Region, to further improve the accuracy. Polling, in theory, enables us to make use of the topology information with the quantity up to $O(n^4)$ provided by CVD for localization, while a conventional CVD scheme can use only O(1) such information. The third part, through simulations, shows how to use the qADC (quasi Analog-to-Digital Conversion) strategy to handle signal errors. Combined with Polling and qADC, a CVD scheme can provide a simple, robust and powerful solution to the wireless network localization. Some of our findings and methods may also contribute to the field of computational geometry its own.

Index Terms—Localization, complete Voronoi diagram, mirror image distribution, polling, wireless networks.

1 Introduction

Location awareness is considered fundamental to wireless applications because in many situations the information collected and communicated by devices is meaningful only in conjunction with the location knowledge. Many mathematical models or methods have been employed to address the localization issue. As an example, in the well-known trilateration model, one can pinpoint the unique position by solving three quadratic equations with two unknowns if we know the location of three anchor nodes. However, there are still some models whose characteristics are not well-understood. In this work, we try to understand a typical localization method based on Complete Voronoi Diagram (CVD) localization model (see Fig.1 for illustration).

In Fig.1a, we uniformly and randomly deploy n beacons (a.k.a. anchors) in a network region K (a square with side length 100 meters in this example) and we want to compute the location of wireless nodes whose positions are not shown in the figure. Assume that we can compute the distance from a wireless node to some anchor nodes in the network. Then using the proximity relationship, the global geometry region will be partitioned into many subregions. When the proximity relationship is simply comparison of the Euclidean distances from the wireless node to the set of anchor nodes, the region is partitioned into Voronoi diagram [30], where each subregion corresponds to one anchor node, denoting that the wireless nodes in this region is closest to this specific anchor node.

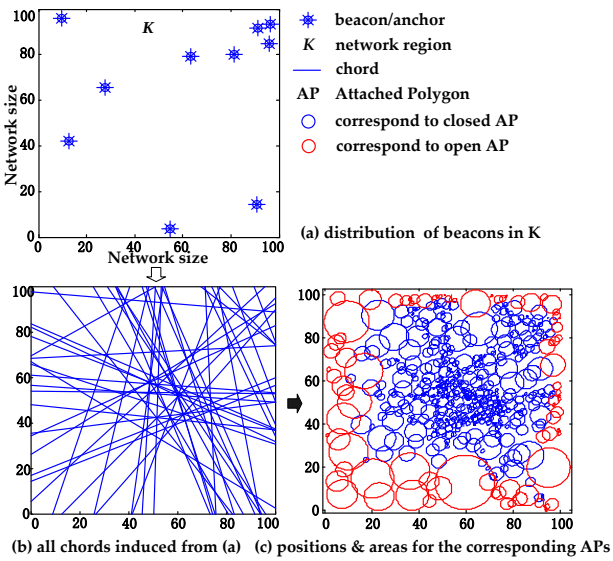

Fig. 1. CVD and its central tendency

In Fig.1b, we compute the perpendicular bisectors of

The first version of this paper was sent to TMC in 2008.

- *Gang Lu, Xiaoming Wang, Xiaojun Wu and Yumei Zhang are with Key Laboratory of Modern Teaching Technology, Ministry of Education, the School of Computer Science, Shaanxi Normal University, Xian, China, 710062, Engineering Technology Center for Environmental Perception and Information Processing, Shaanxi Normal University, Xian, China. E-mail: goforlg@126.com, {wangxm, wythe, zym0910}@snnu.edu.cn*
- *Mingtian Zhou is with the School of Computer Science and Technology, University of Electronic Science and Technology of China, Chengdu, China 610054. E-mail: mtzhou@uestc.edu.cn*
- *Xiang-Yang Li is with the College of Computer Science and Technology, University of Science and Technology of China, China, Department of Computer Science, Illinois Institute of Technology, IL,U.S., Department of Computer Science and Technology, and School of Software, Tsinghua University, Beijing,China. Email: xli@cs.iit.edu; URL: www.cs.iit.edu/~xli.*

Manuscript received (insert date of submission if desired). Please note that all acknowledgments should be placed at the end of the paper, before the bibliography.

all beacon pairs. *K* is thus divided by chords (the intersections of bisectors and *K*) into many small polygons and each unknown wireless node will decide for which polygon it should belong to according to some physical properties of the signals received from anchors (we do not consider signal errors at this point). The rule is as following: the perpendicular bisector joining two anchors, say A and B respectively, divides the plane into two half planes. And an unknown node, say u, compares the RSS_A (Received Signal Strength of beacon A) with RSS_B. If u finds that $RSS_A > RSS_B$, then u knows it is of close proximity to A. Thus u decides it should belong to the half plane which contains A. This process continues until all the beacon pairs are checked out. Finally, u will get an intersection of all the half planes and *K*, which is a Polygon Attached to u (symbolized as AP_u), and take the centroid of AP_u as its position estimate (Note: CVD schemes welcome all measurements changing roughly monotonically with the distance other than RSS. We will discuss this issue in section 7).

The graph in Fig.1b is called the Complete Voronoi Diagram (CVD) because of that all materials to form the conventional Voronoi diagram are preserved in the graph (see Fig.11a in section 5.3 for illustration) and the essential similarity between these two kinds of graphs.

No matter what we call it, CVD has already been used for the wireless network localization [40, 42]. In [40], the authors assign each vertex, edge and polygon in CVD a unique sequence (see Fig.2g), and let the unknown node search the sequence table to locate itself. Using RSS, [40] conducts real MICA 2 motes experiments for both indoor and outdoor localization, the results show that it can achieve 3.3 and 2.3 meters level accuracy when 5 references nodes are deployed. In [42], the authors developed the RF-Compass system, which formulates CVD as a convex optimization problem, and use it for the robot navigation. Using multipath profile [43] as the measurement, when four RFIDs are equipped by the target, RF-Compass can pinpoint target center and orientation to the accuracy of 1.28 cm and 3.3° , respectively. Such accuracy is comparable to other state-of-the-art localization systems: ZEE [34] developed a zero-effort solution to crowdsourcing WiFi data for indoor localization and can achieve about 1.2 ~ 2.3 meters accuracy in real world experiments. EZ [33] and RADAR [2] yield 2 and 1.3 meters of localization error, respectively. Using depth-camera sensor, the Kinsight [39] scheme can track household objects with average location error of 13 cm. Using only COTS RFID products, BackPos [26] and Tagoram [18] can achieve the mean accuracy of 12.8 cm and 6.35 cm in real world deployments, respectively.

Although promising in application, CVD's key features are not mathematically characterized by the previously related papers along with its potential not been fully developed, which might prevent us from thoroughly understanding of the rationale behind the CVD localization. We raise following issues to make clear:

Issue 1: why the previously proposed algorithm can achieve such accuracy? In case more or less anchors or different network region sizes are required, to what level of accuracy can we expect? Unless we find the quantitative relationship between anchor number *n*, network size and the accuracy, to answer the question we have to perform experiment for each situation.

Issue 2: What is the optimal time complexity for a CVD scheme? Actually, to localization, SBL [40] consumes $O(n^6)$ time and $O(n^5)$ storage and RF-Compass [42] consumes $O(rank \cdot N^{2.5})$ time. Here *N* is the number of the constraints, which is equivalent to $O(n^2)$ in this paper's symbolic system, thus the time complexity is $O(n^5)$. In this paper we show the optimal time and space complexities of CVD scheme are $\Theta(n^2)$ and $\Theta(n)$, respectively.

Issue 3: Do the previously related algorithms take fully advantage of the topology information that CVD can provide? The answer is no. In fact, using only the information provided by one attached polygon which the unknown node resides in for localization, previously schemes utilize only O(1) CVD's topology information. While the quantity of such information can be $O(n^4)$. This paper designs Polling technique to address this issue. The simulations show Polling can effectively improve the accuracy performance.

Issue 4: mathematical explanations about the fundamental features of CVD are missed in previous papers. Let us go back to Fig.1b. It is obvious that the chords of CVD tend to distribute to the center region of *K* and Fig.1c shows further that the area of a polygon (i.e. AP) in center region is much smaller than that of a polygon in the non-center region — such phenomenon is called the Central Tendency. Can we expect the different subregions of *K* will have different positioning errors under a CVD scheme? If so, why? And how much is it?

This paper tries to provide some understandings about the mathematical properties of CVD and shows how to utilize the topology information to further improve the accuracy performance and to handle the signal errors.

We identify two fundamental questions about CVD and the CVD localization: ***Q1:*** Why Central Tendency? ***Q2:*** What is the quantitative relationship between the number of vertices, chords and faces in CVD? The further questions might be: ***Q3:*** How to test the reasonableness of the theory about Central Tendency? ***Q4:*** To what level of accuracy does a CVD scheme can expect? ***Q5***: What are the optimal time and space complexities for a CVD scheme? ***Q6***: How much topology information can be utilized by a CVD scheme for localization? ***Q7***: Can CVD schemes handle the signal errors?

The answers to the above questions are our contributions to the literature:

A1: The reason behind the Central Tendency is what we referred to as the Mirror Image distribution and its probability density function, i.e. pdf, is $3(R^2 \arccos(h/R) - h\sqrt{(R^2 - h^2)})/(2R^3)$ (see section 4.1 for details). The key insight here is that we will share mirror with our image when we look at the mirror, which is analogous to a pair of beacons sharing their perpendicular bisector.

A2: $m_f = m_c + m_2 - \left(\sum_{t=3}^{m_c} m_t \bullet (t-1)(t-2)/2\right) + 1$. This result is the key to calculate the number of polygons in CVD.

A3: Should the mirror image distribution is reasonable, the average length of a chord must be $\overline{C} = \sqrt{1024 - 9\pi^2} R/16$.

This actually gives us a simple way to test the reasonableness of the theory by simulation.

A4: Any level. The formula is $\bar{d}_{err}=(2\sqrt{\overline{Area}/\pi})/3$. For average overall localization error, $\overline{Area}=\pi \bullet R^2/(0.105n^4-0.334n^3+0.765n^2-0.537n+1)$ and the denominator here is in fact the number of polygons in *K*, which implies that the localization error is inversely proportional to the *n* square. As an example, in a square with side length 100 meters, in theory we can achieve 1 millimeter level accuracy provided that 300 anchors can be deployed — there is no need to worry too much about the anchor number, actually we just need one mobile anchor or a moving antenna because CVD based schemes can be incrementally performed and do not matter synchronization. For average local localization error, see theorem 7 in section 4.2, $\overline{Area}=\pi(qq^2-q^2)/(m_{f\_qq}\text{-}m_{f\_q})$.

A5: It will consume $\Theta(n^2)$ time and $\Theta(n)$ space for an unknown node to locate itself. The optimality lies on the fact that the average edge number of an AP is 4 as $n\rightarrow$ *large* (section 4.2, corollary 2) — which implies that we can calculate the intersection of a half plane and a CVD AP in $\Theta(1)$ time.

A6: Usually O(1) , i.e. its attached polygon (AP), for each unknown node can be used. However, with Polling technique, in theory, we can use all CVD polygons with quantity up to $O(n^4)$ for localization. The insight about Polling is that if an unknown node u takes a wrong place as its estimation, it has a chance to be detected by u's neighbors (including both unknown nodes and anchors) when they try to update their attached polygons according to the received signals from u.

A7: Yes, by qADC strategy, it can. CVD schemes can be robust to the growth of signal errors (with an elegant compromise of its accuracy performance). Since there are large amount of resources (i.e. beacon pairs) can be used for localization, we can drop some of resources whose credibilities are not high enough, or formally, the difference is no more than a threshold of cσ (here σ is the standard deviation of the Gaussian noise distribution, and the proper value of c is 2 according to our simulation results), while still keep the reasonable accuracy.

Our findings and methods may not only just contribute to the field of the wireless network localization, some of them might also contribute to the field of the computational geometry its own.

The rest of this paper is organized as follows. Section 2 introduces related works. Section 3 describes the terminologies, notations and a basic CVD scheme to facilitate our analysis. Section 4 proves the mathematical properties of CVD. Section 5 shows how Polling works. Section 6 proposes the qADC strategy to handle signal errors (which we have to face in real world) and studies accuracy performance through extensive simulations. Section 7 remarks some features of CVD based schemes. Section 8 concludes our work.

2 RELATED WORKS

A localization scheme usually consisted of two stages: the **measurement stage** in which the raw measurement information such as signal strength or traveling time [1] is collected; and the **retrieving stage** in which the desired location knowledge is revealed and refined through some mathematical computation models such as triangulation, multilateration, Bayesian methods [27], neural networks [28], etc. It seems that the accuracy performance ultimately limited by the underlying signal technology employed in the measurement stage. In this section we mainly group the related works according to the different kinds of measurements.

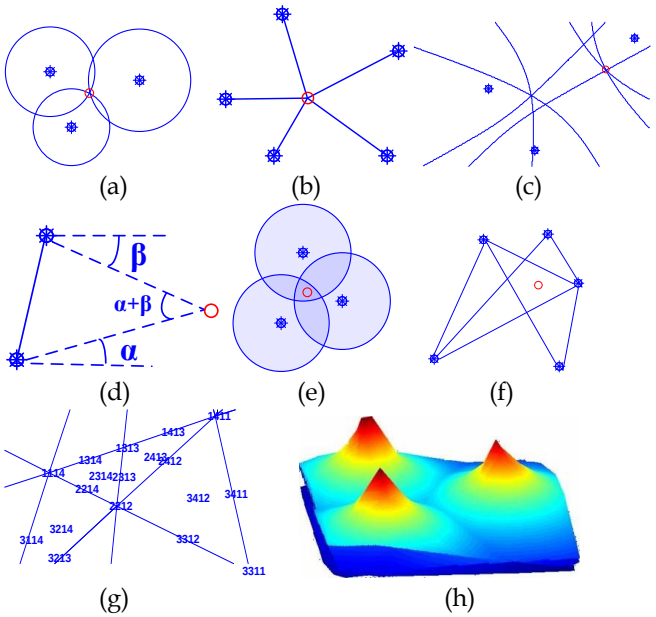

Fig. 2. Illustration for the principles of some location computing models. **(a)** Trilateration [3], [10], [44]: unknown position can be revealed by calculating the unique intersection of 3 circles. **(b)** Multilateration [11], [12], [13]: the unknown position can be estimated by minimizing the differences between the estimated distances and the measured distances (through some Maximum Likelihood methods, for example MMSE—Minimum Mean Square Estimate). **(c)** Hyperbolic localization [7], [8], [37]: unknown node lies at the intersection of two hyperbolas (at least three anchors or two sets of hyperbolas are required). **(d)** Triangulation [9], [17]: with trigonometry laws of sines and cosines, the desired position can be revealed. **(e)** Proximity localization [21]: choose the center of the overlapping areas as the estimate. **(f)** PIT (Point-In-Triangulation test) [22]: if no neighbor is further from or closer to the three anchors simultaneously, the unknown node assumes it is inside the triangle. Choose the center of the triangles intersection as the position estimate. **(g)** Location sequences for a four-reference-node space division (anchors are labeled with 1, 2, 3 and 4, respectively) [40]: By selecting a nearest sequence from the sequence table, unknown node localizes itself to the point that this sequence represented. **(h)** Radio Map [2], [33], [34], [41]: also known as the fingerprint method. By searching the most likely matching signal pattern in database, which is usually constructed in advance, this method can pinpoint the target with acceptable accuracy.

2.1 RSSI

RSSI (Received Signal Strength Indicator) implemented with RF transmitters and receivers [2], which is one of the simplest approach because most radio communication

devices come with built-in RSS indicator hardware.

Combined with a channel model, RSSI can be used to provide distance estimate [3]. In a 2D region, three (or more) anchors are required to locate an unknown node — the corresponding process is called the trilateration (or multilateration). See Fig.2a and Fig.2b for illustration.

Although measuring RSS is available in most sensor nodes, such techniques have to face some baptisms of practice [4], [7], such as obstacles, multipath effects and background noise, which often lead to large errors in distance evaluation. In [13], the bias and variance issues in estimating distance from RSS under log-normal shadowing channel model are considered. The authors show that both the bias and the MSE (Mean-Square Error) of MLE (Maximum Likelihood Estimator) grow exponentially with the noise power. Therefore the RSSI technique, especially the one that directly mapping RSSI values to Euclidean distances is not accurate and its adoption should be confined to the applications require only coarse estimation.

The active badge project [10], developed in AT&T Cambridge, employs a centralized service to locate people who wear badges (infrared sensors) that transmitting signals. The RADAR [2] system uses RF signal strength receiving from three fixed stations to track user locations within a building. SpotOn project [31] developed a fine grained tagging technology based on RF signal strength analysis for three dimensional location sensing.

AHLos (Ad-Hoc Localization System) [11] , consisted of two phases (ranging and estimation) and three multilateration processes (atomic, iterative and collaborative), have been employed to obtain the position estimates. Based on AHLos, the n-hop multilateration primitive [12] uses the Kalman Filter to set up a gradient which enables nodes to estimate their globally optimal positions by performing the computation locally (some beacons need to be deployed to the network edges).

APIT [22] employs an area-based approach named PIT (Point-In-Triangulation test) to perform location estimation. In PIT, unknown node tests whether it lies in the triangles formed by audible beacons and use the center of gravity of the intersection of all these triangles as its estimate. See Fig.2f for illustration. The unknown node assumes that it is inside/outside a triangle formed by three anchors by checking whether a neighbor has consistently larger or smaller signal strengths measured from these three anchors.

A sequence based localization (SBL) scheme has been introduced by Kiran Yedavalli and Bhaskar Krishnamachari [40]. The key idea of their technique is the distinct 2D space division induced by the perpendicular bisectors joining each pair of anchors. As shown in Fig.2g, each region, edge and vertex are all labeled with unique location sequence according to their distances to the anchors. Combined with some distance rank metrics, the authors developed a localization scheme which is robust to signal errors. The systematic simulations and a set of real mote experiments are performed, and the results show that SBL is a promising technique which provides better/comparable accuracy than/to some other state-of-the-art RSS based localization schemes. By showing the number of feasible sequences is $O(n^4)$, where n denotes the anchor number, the authors proved that their approach consumes $O(n^6)$ time and $O(n^5)$ storage. To our knowledge, SBL is one of the first utilizations of CVD.

2.2 TOA

In a TOA (Time-of-Arrival) based scheme [15], given the speed and propagation time of the signal, the range information between transmitters and receivers can be estimated. There are two kinds of TOA: one-way TOA and two-way TOA. The former needs a common clock to be projected into the two nodes in order to calculate the traveling time. Using the round-trip time (RTT), the two-way TOA eliminates the need of a common time reference (however, the response delay and the clock offset sometimes still cause troubles). Besides synchronization, a good LOS (Line-Of-Sight) is also required by a TOA scheme.

In GPS [5] denied environments, especially for indoor and short-distance applications, the UWB [36] (Ultra WideBand, standardized in IEEE 802.15.4a) technique recently stands out to be a promising one in high resolution range due to its particular characteristic of improved time of flight resolution, improved capability of penetrating materials, low-power and low-cost implementation. Although centimeter-level distance resolution can be achieved, many challenges still remain for UWB technique to address: multipath components, obstacles, interference, clock drift, etc. Please see [32], [35], [36] for more details.

2.3 TDOA

The most famous TDOA [8], [37] (Time Difference of Arrival) approach is GPS, which can provide a good estimate with the error less than few meters. And the most successful application using GPS might be the Google Maps, which can bring tremendous convenience to people in their daily life.

In principle, localization using TDOA can be realized by intersecting the hyperbolas which corresponds to the distance differences between the unknown node and various anchors. See Fig.2c for illustration.

The following two schemes are commonly used in TDOA computation: the first one lets synchronized anchors broadcast beacons and then unknown node measures TDOA; the second one lets unknown node broadcast signal and then the synchronized anchors compute TDOA (an information exchanging protocol between anchors is required). However, sometimes TDOA can be implemented in an alternative way: sender is equipped with special hardware that can simultaneously emit different kinds of signals (ultrasonic and RF), and receiver computes TDOA via the measured arrival times [8].

Similar to TOA, TDOA also requires precise synchronization (among reference nodes to insure a same timing offset), which might limit its usage in energy-restricted sensor networks. NLOS (Non-Line-Of-Sight) is another important issue for TDOA (and TOA) schemes to address.

Using smart phone as a supplementary to GPS to fur-

ther improve the accuracy [6], [14] is an emerging line of research in the field.

2.4 AOA

As an extension of TOA and TDOA, AOA (Angle of Arrival) schemes [9] derive location knowledge from the geometric angles between objects. Given one side length and two angles of a triangle which formed by an unknown node and two anchors, the position of the unknown node can be unambiguously found using trigonometry. See Fig.2d for illustration. In practice, the anchors mentioned above can be different antennas in one anchor, and the angle information is obtained by measuring the difference of the signals' phases [18], [26].

One of the significant drawbacks of AOA schemes is that the measuring angle errors grow rapidly with the increasing distance between unknown nodes and anchors. Another issue calls challenge for AOA is NLOS problem.

2.5 Connectivity and Proximity: Range-free

DV-hop [17] is a typical rang-free scheme in which beacons flood their location information to the network and unknown nodes estimate their positions through some kinds of triangulation methods. DV-hop belongs to APS (Ad-hoc Positioning System) [9] which combines the distance vector with some hybrid methods to estimate the location in presence of measurement errors.

Based on connectivity and pairwise angles between nodes, the convex position estimation [20] formulates the position estimation as a linear or semidefinite programming. Simulations presented in [20] show that a quick solution for the problem of network localization with several hundred nodes is possible.

The Multi-dimensional Scaling MAP (MDS-MAP) [23] uses only the connectivity information for localization and consisted of three stages: (1) the all-pairs shortest paths algorithm is performed to obtain a distance matrix; (2) MDS technique is used to derive the node locations that fit the distances; (3) the known knowledge (beacons) is used to refine the estimations. MDS-MAP can also be performed in a range-based fashion.

The Centroid [21] uses proximity information to locate nodes: unknown nodes firstly determine their proximities to anchors and then estimate their positions by calculating the overlapping regions (see Fig.2e).

2.6 Radio Map

Instead of determining the distances between user and the anchors and triangulating the user location, radio map based schemes determine the location by comparing the measured RSSI (or other measurements) values to a signal pattern database [2]. Such database is usually constructed in an offline phase and contains the measured RSSI patterns at certain locations. In this way the channel modeling for the complex radio signal propagation is avoided. However, the offline phase is quite laborious, and the more important problem is that those patterns varying with time and vulnerable to environmental dynamics. Some online determinations for the training values have been proposed [41] to improve the reliability of fingerprints and to cope with the time-varying nature of radio environments. And much effort goes into the sites survey process removing research [33], [34].

Gauss-Markov models, Bayesian and Kalman filter etc. are commonly used math tools in the retrieving stage of the radio map schemes.

2.7 Multipath Profile

J.Wang et al. [42] proposed RF-Compass system for robot navigation and can achieve centimeter-scale accuracy. RF-Compass equipped the robot and the target object with some RFIDs and then use perpendicular bisectors generated from those RFIDs to perform space partition. RF-Compass uses a newly developed technique called Multipath Profile [43] (i.e. all the paths along which a sender's signal propagates) to measure the relative distance between pairs of RFIDs, and correctly narrows down the overlaying partitions. The Multipath Profile technique uses a synthetic aperture radar (SAR) created via antenna motion to extract multipath profile and then adapt dynamic time warping (DTW) to estimate proximity of two RFIDs. Using the coordinate transformation and two or more RFIDs, RF-Compass can find the location and the orientation of the target object at the same time. RF-Compass formulates its localization task as a convex optimization problem and designs an iterative algorithm to solve it.

RF-Compass is also one kind of utilizations of CVD: the RFIDs on robot actually equivalent to the anchors and the RFIDs on target equivalent to the unknown nodes.

2.8 CSI (Channel State Information)

FILA [44] might be the first work that using CSI for localization. CSI can estimate channel in subcarrier level while RSSI in packet level. FILA first collects CSI and computes a weighted value as CSI_{eff} and then applies some pretrained parameters to a formula $d=f(CSI_{eff})$ to calculate distance between the receiver and the sender. In Lab, FILA can achieve meter level accuracy.

NomLoc [45] use nomadic access points and CSI for indoor localization, and can achieve meter level accuracy.

2.9 Hybrid Measurements

Different measurements [19], [27], [28] such as vision [29], [39], acoustic, RF etc., can be combined together to acquire the positioning information.

2.10 Network Localization

In a network, some nodes know their locations in advance. We can propagate such knowledge across the network and guide other nodes to determine their locations according to some protocols. Such process is called the network localization [24]. If we call previously mentioned methods, as shown in Fig. 2, the single localization, then the network localization can be regarded as the social localization, which means the nodes may help others to localize themselves.

Network localization is one of the most fundamental issues about the localization. In [24], the authors raised some basic questions about network localization: What are the conditions for unique network localizability?

What is the computational complexity of network localization? Applying the concept of grounded graphs and the graph rigid theory, they obtained some profound results. They showed that a network with a biconnected grounded graph is uniquely localizable if two-hop neighbors are connected and the complexity of network localization belongs to NP-hard. Zheng, et al [16] further proposed an optimal distributed algorithm to recognize all one-hop localizable nodes by using wheel graph.

Another cornerstone of network localization is how to balance the accuracy with resource cost (e.g. energy or time consumption) when exploring the correlation among network nodes (positions and links). This issue is quite important for contemporary mobile and real-time applications. One of the most recent results has been reported in [25]. The authors formulate the network localization as the optimization problem using least squares method and apply canonical duality theory for non-convex analysis and global optimization. Their results show the general network localization problem is not NP-hard unless its canonical dual problem has no solution. Yuan, et al [38] proposed a unifying optimization framework for power allocation in both active and passive localization networks. Though a lot of efforts have been put into this line of research, to our knowledge, the issue is still open. How the uncertainty propagates, to what level of accuracy can we expect … there is so much more left of it for us to explore.

3 PRELIMINARIES

3.1 terminologies and notations

TABLE 1
Summary of terminologies and notations

beacon	or anchor, i.e. a node with known position
unknown node	a node whose position is unknown
K, ∂K, R	K is a 2D network region and anchors uniformly and randomly reside in it. ∂K denotes the boundary of K. When K is a disk, R denotes its radius. CVD will stretch out to the whole 2D plane, and K is called the *Kernel* of CVD
n	the number of beacons
chord	a segment which is the intersection of a line and K.
AP	Attached Polygon. Assume K is divided by chords into many small polygons and u is a node inside K. By $\boldsymbol{AP}_u$, we mean the polygon that contains u. Without the subscript, AP just means a polygon
open/closed AP	AP with at least one/no edge lies on ∂K
m_f	the number of APs in K
m_c	the number of chords in K
x_t $(t \geq 1)$	a point with total $t \geqslant 1$ lines passing through it. In Fig.3a, there are two x_2, three x_3 (enclosed with red circle) and infinite x_1.
m_2	is the number of events that different pair of lines passing through a common point. Fig.3a has 2 x_2 and 3 x_3, so $m_2 = 2 + 3\binom{3}{2} = 11$.
m_t $(t \geq 3)$:	is the number of x_t $(t \geq 3)$.
	In Fig.3a, m_3=3, and m_4, m_5 …=0
Mirror Image	a mirror image of an object S, denoted by $M(S)$, mirroring S with respect to a given axis; this axis is called the mirror. See Fig.3b.
$H(sign(A))$ $H(-sign(A))$	assume line L divides the plane into two half planes and A is a point not lie on L, then by $H(sign(A))$ (or $H(A)$) we mean the half plane that contains A and $H(-sign(A))$ (or $H(-A)$) the opposite half plane

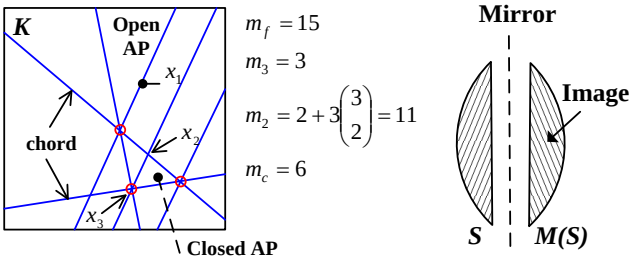

Fig. 3. Illustration for the terminologies and notations

For simplicity, we use RSSI as the measurement and unless otherwise specify, we always assume: the signal strength roughly decreases with distance; all nodes uniformly and randomly distributed in K; all powers are in dBm and all distances are in meter.

3.2 BCVD—a Basic CVD localization scheme

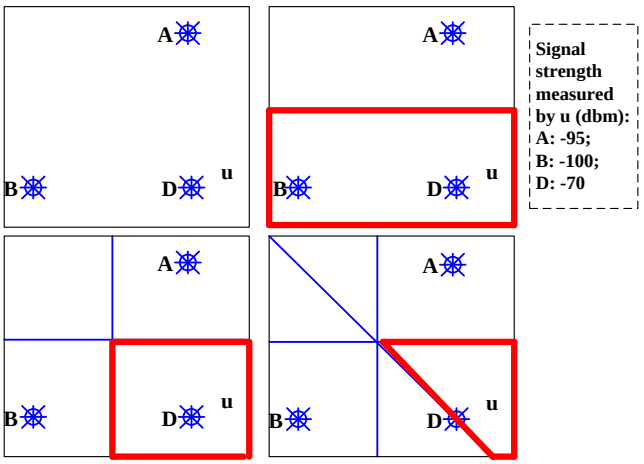

Fig. 4. Illustration for BCVD. In the upper left corner of Fig.4, unknown node u sets its initial AP as a square; in the upper right corner, based on the strengths of the received signals from anchor A and D (the values are shown right to the Figure), u finds that it is proximity to D. So u computes the perpendicular bisector joining A and D to divide the plane into two half planes, and updates its AP as AP_u=H(sign(D))⋂ AP_u. Finally, u gets AP_u (the red colored polygon) as shown in the lower right corner of Fig.4 and locates itself to the centroid of AP_u.

See Fig.4, the idea of BCVD is quite simple: unknown node u computes perpendicular bisectors of all audible anchor pairs and at each computation u decides for which half plane it should belong to according to the received signals. The pseudo code of BCVD is given bellow.

Input: *Anchors, UnknownNodes, K, TransPower.*
Output: position estimates of *UnknownNodes.*
BCVD (*Anchors, UnknownNodes, K, TransPower*)
1) **INITIALIZE** (*UnknownNodes,K*)

```
2)  MEASUREMENT(Anchors, UnknownNodes, TransPower)
3)  for each v ∈ UnknownNodes
4)      UPDATE(v)
5)  for each v ∈ UnknownNodes
6)      v.EstimatedPosition ← centroid(v.AP)
7)  return position estimates of UnknownNodes
INITIALIZE (UnknownNodes, K)
1)  for each v ∈ UnknownNodes {
2)      v.AP ← K
3)      v.EstimatedPosition ← ∅ // empty set
4)      v.SL ← ∅ // Signal List
5)  }
6)  return UnknownNodes
MEASUREMENT (Anchors, UnknownNodes, TransPower)
1)  for each u ∈ Anchors, using TransPower, broadcast Beacon_u to network region
2)      for each v ∈ UnknownNodes && u is audible
        //Beacon_u includes the u's position, index and RSSI
3)          v.SL ← v.SL ∪ Beacon_u
4)  return UnknownNodes // with updated signal list
UPDATE (v)
1)  n ← number of beacons in v.SL
2)  Sort v.SL to descending order in accordance with the RSS value.
3)  for i = 1 to n-1 {
4)      A ← v.SL(i) //selects one anchor
5)      for j = i+1 to n {
6)          B ← v.SL(j) // selects another anchor
7)          Divides the plane into two half planes by the perpendicular bisector joining A and B. Choose the half plane in which A resides as the H(sign (A)).
8)          v.AP ← v.AP ∩ H(sign (A))
9)      }
10) }
11) return v//with its updated AP
```

4 PROPERTIES OF CVD

4.1 Fundamental Properties of CVD

A. Central Tendency and the Mirror Image Distribution

Definition 1. The Mirror Image distribution is the distribution of chords in the *Kernel* of CVD (See Fig.1b).

Theorem 1. Assume all anchors uniformly distributed in K and K is a disk (including its whole interior region) with radius R. Let h denote the shortest distance from the disk center to an arbitrary chord, the *pdf* (probability density function) of Mirror Image distribution, say f_M, is:

$$f_M = \begin{cases} \frac{3}{2} \bullet \frac{R^2 \arccos(h/R) - h\sqrt{(R^2-h^2)}}{R^3} & 0 \le h < R \\ 0 & otherwise \end{cases} \quad (1)$$

Proof. See Fig.5a. S is a bow of area $S = R^2\arccos(h/R) - h\sqrt{R^2-h^2}$, by symmetry we only need to consider an arbitrary chord C as shown in Fig.5a. Regarding C as the mirror, C will be shared by every point in S and its mirror point in $M(S) \bigcap K = M(S)$. Using area as a measure for the number of chords and let a positive constant $\Delta h \to 0$ and $X \in [0,R)$, we can find the cumulative distribution function $F(h)$ as:

$$F(h) = \Pr\{X \le h\} = \frac{\Delta h}{\Delta h} \bullet \frac{\sum_0^h S}{\sum_0^R S} = \frac{\int_0^h S \bullet dh}{\int_0^R S \bullet dh}$$
$$= \frac{3h \bullet \arccos(h/R)}{2R} - \frac{\sqrt{R^2-h^2}}{R} - \frac{h^2\sqrt{R^2-h^2}}{2R^3} + 1 \quad (2)$$

Differentiating with h on both sides of (2) and noting that $0 \leqslant h < R$ will complete the proof. ■

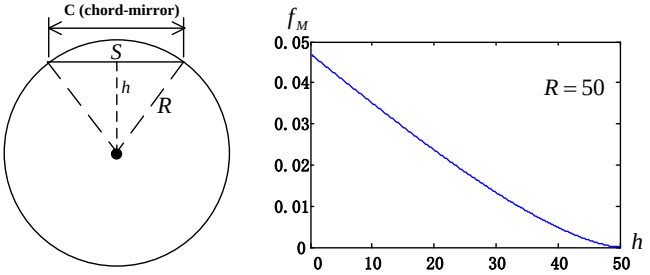

(a) Illustration for theorem 1 (b) the probability density function f_M

Fig. 5. The mirror image distribution

Fig.5b implies the probability of an arbitrary chord to be tangent to a concentric circle of K with smaller radius is higher than the probability of the chord to be tangent to a concentric circle with larger radius. So there are more chords in the center region and a polygon there has more chance to be divided into smaller ones—such is the rationale behind the central tendency.

B. Relationship between m_f, m_t and m_c

Theorem 2. Let K be a convex region and no 4 or more anchors lie on a common circle, then in CVD we have

$$m_f = m_c + m_2 - m_3 + 1 \quad (3)$$

In case 4 or more anchors may lie on a common circle, the general form of theorem 2 is:

Theorem 3. Let K be a convex region, in CVD we have

$$m_f = m_c + m_2 - \left[\sum_{t=3}^{m_c} m_t \bullet \frac{(t-1)(t-2)}{2}\right] + 1 \quad (4)$$

Should theorem 3 can be proved, theorem 2 then follows.

Proof of theorem 3. It is easy to verify that when m_c=0, 1 and 2 the equation (4) holds. Suppose (4) holds for m_c=k, we now consider adding the k+1th chord to K.

Imagine the k+1 chord passing through K from one side (a start-point, abbreviated by s.p.) to another side (an end-point, abbreviated as e.p.), we can observe the following facts as shown in table 2.

TABLE 2

The March of the k+1th Chord through K

Arriving at	Δ_{left}	Δ_{right}			
	m_f	m_c	m_2	$-\sum_{t=3}^{m_c} m_t \bullet (t-1)(t-2)/2$	1

s.p.	0	0	0	0	0
x_1	+1	0	+1	0	0
x_2	+1	0	+2	$-(3-1)(3-2)/2=-1$	0
⋮	⋮	⋮	⋮	⋮	⋮
x_k	+1	0	+k	$-[k(k-1)-(k-1)(k-2)]/2$ $=1-k$	0
e.p.	+1	+1	0	0	0

Note: Δ_{left} / Δ_{right} means the difference in the left-/right- hand side of equation (4).

Checking whether $\Delta_{left}=\Delta_{right}$ from the s.p. row to the e.p. row of table 2 will complete the proof. ■

In fact, the probability that 4 or more anchors lie on a common circle is zero given the random distribution of anchors. So the most often used relationship in practice is equation (3).

4.2 Advanced Properties of CVD

A. Average chord length

Corollary 1: assume *K* is a disk with radius *R*, the average length of a chord, denoted by $\overline{C}$, in *K* is:

$$\overline{C}=\frac{\sqrt{1024-9\pi^2}}{16}R \tag{5}$$

Proof. The weighted position of a chord in *K* is $\overline{h}=\int_{-\infty}^{\infty}hf_M dh=\frac{3\pi}{32}R$, which gives $\overline{C}=2\sqrt{R^2-\overline{h}^2}$. ■

Note: We can verify Mirror Image Distribution by $\overline{C}$ should the theorem 1 is reasonable. Actually, we run the simulation one million times to calculate $\overline{C}$ and in each run we let different number of anchors randomly and uniformly distributed in *K*. The result shows that the average length of *C* is 1.91*R*, exactly what the equation (5) tells. Although the simulation is not necessary, the result can strengthen our confidence about the reasonableness of the mirror image distribution.

B. Two event probabilities of CVD

Theorem 4. Let *in2* denote the event that a intersection of two arbitrary perpendicular bisectors of CVD lies inside *K* (*K* is a disk including whole interior region), the probability of *in2*, say Pr{*in2*}, is approximately 0.84.

Proof. Taking the center of *K* as origin, by symmetry, we only need to consider the intersections which lie on a half line from the origin O to $b\to\infty$ as shown in Fig.6.

In Fig.6a, A is the intersection of line L and x-axis; *x* is the distance between O and A; $L\cap K$ is a chord which divides *K* into two parts and the smaller one, denoted by *S*, is a bow. Without ambiguity, *S* is also used to denote bow's area. Imagine we use A as a center and rotate L, as we do in the proof of the mirror image distribution, the sum of area S can be used as a measure for the number of chords that passing through A (note that the each point pair is unique when we rotate L) .

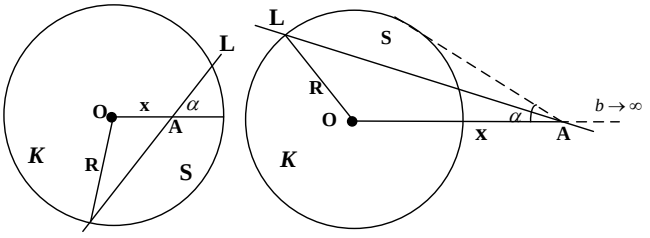

(a) A lies inside *K* (b) A lies outside *K*

Fig. 6. Illustration for the proof of Pr{in2}

Let *I* be a measure for the number of intersections which lie on x-axis inside *K* (from 0 to R) and note that the chords generating at any arbitrary angle α (with respect to x-axis) are actually a beam of overlapping lines, we have

$$I\overset{\sim}{\propto}\frac{1}{2}\sum_{x=0}^{R}\left[\left(\sum_{\alpha=0}^{\pi}S\right)^2-\sum_{\alpha=0}^{\pi}S^2\right]\approx\frac{1}{2}\sum_{x=0}^{R}\left(\sum_{\alpha=0}^{\pi}S\right)^2=2\sum_{x=0}^{R}\left(\sum_{\alpha=0}^{\pi/2}S\right)^2 \tag{6}$$

By $\overset{\sim}{\propto}$ we mean the left-hand side of $\overset{\sim}{\propto}$ is approximately proportional to the right-hand side of $\overset{\sim}{\propto}$.

Let *J* be a measure for the number of the intersections which lie on x-axis outside *K* (from R to $b\to\infty$, see Fig.6b), through a similar process we have

$$J\overset{\sim}{\propto}\sum_{x=R}^{b\to\infty}\left[2\left(\sum_{\alpha=0}^{\arcsin\frac{R}{x}}S\right)^2-\sum_{\alpha=0}^{\arcsin\frac{R}{x}}S^2\right]\approx 2\sum_{x=R}^{b\to\infty}\left(\sum_{\alpha=0}^{\arcsin\frac{R}{x}}S\right)^2 \tag{7}$$

Here $S=R^2\arccos(x\sin\alpha/R)-x\sin\alpha\sqrt{R^2-x^2\sin^2\alpha}$.

The desired probability can be written as:

$$\Pr\{in2\}\approx\frac{I}{I+J}\approx\frac{\int_0^R\left(\int_0^{\pi/2}Sd\alpha\right)^2dx}{\int_0^R\left(\int_0^{\pi/2}Sd\alpha\right)^2dx+\int_R^b\left(\int_0^{\arcsin(R/x)}Sd\alpha\right)^2dx} \tag{8}$$

The result of (8) can be numerically evaluated. ■

Theorem 5. Let *in3* denote the event that a common intersection of three perpendicular bisectors of CVD lies inside *K* (*K* is a disk including its whole interior region), the probability of *in3*, say Pr{*in3*}, is approximately 0.74.

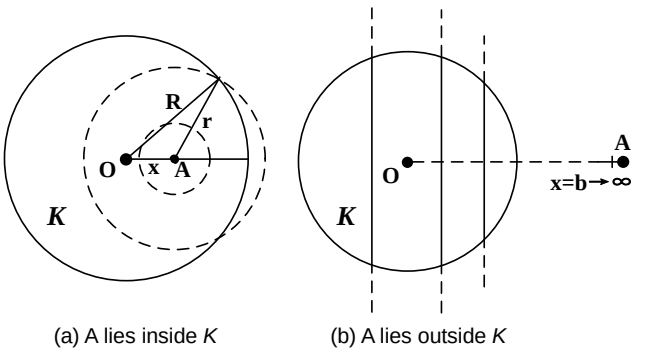

(a) A lies inside *K* (b) A lies outside *K*

Fig. 7. Illustration for the proof of Pr{*in3*}

Proof. Noting that the common intersection of three perpendicular bisectors must be the circumcenter of the corresponding triangle, by symmetry of *K* we only need to consider the circumcenters which lie on x-axis (from O to $b\to\infty$, please see Fig.7).

Let *I* be a measure for the number of triangles

whose circumcenters lie on x-axis inside K and J for that of outside K. We use the length of an arc which is the intersection of a circle (centered at A, see Fig.7a for illustration) and K as a measure for the number of points that lie on the arc. Since every distinct combination of three points forms a unique triangle, we have

$$I \propto \sum_{x=0}^{x=R}\left[\sum_{r=0}^{r=R-x}\pi^3 r^3 + \sum_{r=R-x}^{r=R+x} r^3(\arccos\frac{x^2+r^2-R^2}{2xr})^3\right] \quad (9)$$

When x>>R (x is the distance from the origin to point A), as shown in Fig.7b, the intersection arc (centered at A) can be seen as a segment. Thus, the average value of J, denoted by $\overline{J}$, can be given by

$$\overline{J} \propto 2\sum_{x=0}^{x=R}\left(R^2-x^2\right)^{3/2} \quad (10)$$

From Set Theory we know that two segments have the same cardinality. Let *card*(*in*) denote the number of points that lie on x-axis inside K (from the origin to R) and *card*(*out*) the number of the points that lie on x-axis outside K (from R to $b\to\infty$), then *card*(*in*)=*card*(*out*). The desired probability can be written as

$$\Pr(in3) \approx \frac{I/card(in)}{I/card(in)+J/card(out)} = \frac{\overline{I}}{\overline{I}+\overline{J}}$$

where $\overline{I}$ is the average value of I. Instead of directly calculate $\overline{I}$, we compute a weighted position of A as:

$$\frac{\int_0^R\left(\int_0^{R-x}\pi^3 r^3 dr + \int_{R-x}^{R+x} r^3\left(\arccos\frac{x^2+r^2-R^2}{2xr}\right)^3 dr\right)xdx}{\int_0^R\left(\int_0^{R-x}\pi^3 r^3 dr + \int_{R-x}^{R+x} r^3\left(\arccos\frac{x^2+r^2-R^2}{2xr}\right)^3 dr\right)dx} \approx 0.34R \quad (11)$$

The result of (11) is obtained through some numerical processes. Then by some manipulations, the value of the desired probability can be found. ■

C. The average overall localization error

Definition 2. Suppose the average area of an AP in K (K is a disk with its whole interior region) is S, then the max average localization error is defined as $\overline{d}_{err}^{\max} = 2\sqrt{S/\pi}$ and the average localization error is defined as $\overline{d}_{err} = (2\sqrt{S/\pi})/3$.

(Reason for the definition: Regarding AP as a circle with area S and AP's centroid the circle center, we use the diameter of this circle as the $\overline{d}_{err}^{\max}$ and the average distance from an arbitrary point in circle to the center as $\overline{d}_{err}$.)

Theorem 6. Suppose all anchors are uniformly and randomly distributed in K (K is a disk including its whole interior region), the average overall localization error of a CVD scheme (e.g. BCVD) can be expressed as:

$$\overline{d}_{err}^{\max} = \frac{2R}{\sqrt{0.105n^4-0.334n^3+0.765n^2-0.537n+1}} \quad (12)$$

$$\overline{d}_{err} = \frac{2R}{3\sqrt{0.105n^4-0.334n^3+0.765n^2-0.537n+1}} \quad (13)$$

Proof. In CVD, n beacon nodes will induce $n(n\text{-}1)/2$ bisectors and $n(n\text{-}1)(n\text{-}2)/6$ triangles. Applying theorem 4 and theorem 5 to equation (3) and noting that all the bisectors can further induce $(n/4)(n\text{-}1)(n(n\text{-}1)/2\text{-}1)$ intersections, we have

$$m_f = \frac{n(n-1)}{2} + \Pr\{in2\}\frac{n(n-1)}{4}\left(\frac{n(n-1)}{2}-1\right) - \Pr\{in3\}\frac{n(n-1)(n-2)}{6} + 1 \quad (14)$$
$$\approx 0.105n^4 - 0.334n^3 + 0.765n^2 - 0.537n + 1$$

The average area of an AP is

$$\overline{Area}_{AP} = \pi \bullet R^2 / m_f \quad (15)$$

By definition 2 the desired results can be obtained. ■

Corollary 2. The average edge number of an AP in K is:

$$\overline{N}_{edge} = \frac{n(n-1)(3n+4)(7n-4)}{50\times(0.105n^4-0.334n^3+0.765n^2-0.537n+1)} \quad (16)$$

and $\overline{N}_{edge} = 4 \ \ as\ n \to \text{large}$

Corollary 2 can be verified easily and we omit its proof.

D. The average local localization error

Lemma 1. Theorem 2 holds for any convex region in CVD. See table 2, the correctness of Lemma 1 is straightforward.

Lemma 2. There are m_{f_q} faces (polygons) in a concentric circle q (q is also used for its radius) of K, and

$$m_{f\_q} = m_{c\_q} + m_{2\_q} - m_{3\_q} + 1$$
$$\begin{cases} m_{c\_q} = F_c(q) \bullet n(n-1)/2 \\ m_{2\_q} = F_2(q) \bullet \Pr\{in2\} \bullet n(n-1)(n(n-1)-2)/8 \\ m_{3\_q} = F_3(q) \bullet \Pr\{in3\} \bullet n(n-1)(n-2)/6 \end{cases} \quad (17)$$

Here $F_c(q)$, $F_2(q)$ and $F_3(q)$ are the distributions of m_c, m_2 and m_3 in q, respectively. And by distribution we mean the ratio of the number in q to the corresponding number in K. As an example,

$$F_c(q) = \frac{number\_of\underline{c}hords\_pa\underline{s}ing\_throu\underline{g}h\_q}{number\_of\underline{c}hords\_pa\underline{s}ing\_throu\underline{g}h\_K}.$$

To save space, we show the expressions of these three distributions in proof.

Proof. By Lemma 1, we can apply equation (3) to compute m_c, m_2 and m_3 in q. From theorem 4 and theorem 6 we know there are $\Pr\{in2\}n(n\text{-}1)(n(n\text{-}1)\text{-}2)/8$ m_2 in K. According to the definition of $F_2(q)$, m_{2_q} should be m_2 in q. Through two similar analyses, we can prove the correctness of the m_{c_q} and m_{3_q}.

Next, we will show how to compute $F_c(q)$, $F_2(q)$ and $F_3(q)$. For simplicity, we project circle q onto a unit disk with radius 1. In other words, in $F_c(q)$, $F_2(q)$ and $F_3(q)$, q is actually the ratio q/R.

By theorem 1, the ratio of the number of chords that intersecting a concentric circle q to all chords number is $F(h)$. Replacing the tuple (h, R) with (q, 1) yields

$$F_c(q) = 3q \bullet \arccos(q) - \sqrt{1-q^2} - r^2\sqrt{1-q^2}/2 + 1$$

Let f_2 be a measure for m_2 at a point inside K, from theorem 4 we know $f_2 \propto (\sum_{\alpha=0}^{\pi/2} S)^2$. By symmetry, the distribution of f_2 in K is $F_2(q) = \sum_{x=0}^{q} f_2 / \sum_{x=0}^{R} f_2$. Again, we will let R=1. Many ways, such as numerical integration, fitting, etc., can compute $F_2(q)$. As an example, the Taylor polynomial approximation may lead to

$$F_2(q) \approx 0.013q^7 - 0.14q^5 + 0.22q^4 + 0.46q^3 - 1.7q^2 + 2.2q$$

Let f_3 be a measure for m_3 at a point inside K, theorem 5 tells $f_3 \propto \sum_{r=0}^{r=R-x}\pi^3 r^3 + \sum_{r=R-x}^{r=R+x} r^3(\arccos\frac{x^2+r^2-R^2}{2xr})^3$.

By symmetry, the distribution of f_3 in K is $F_3(q)=\sum_{x=0}^{q} f_3/\sum_{x=0}^{1} f_3$. Applying Taylor polynomial approximation we may find

$$F_3(q)\approx 0.059q^5-0.87q^4+0.25q^3-3.3q^2+2.6q \quad \blacksquare$$

Theorem 7. Let q, qq be two concentric circles (of K) with radius of q and qq, respectively, and $q<qq$. The average localization error for subregions lie between these two circles (or annulus) is

$$\bar{d}_{err}^{local}=\frac{2}{3}\sqrt{\frac{\pi(qq^2-q^2)}{m_{c\_q\_qq}+m_{2\_q\_qq}-m_{3\_q\_qq}}}$$

$$\begin{cases} m_{c\_q\_qq}=(F_c(qq)-F_c(q))\bullet n(n-1)/2 \\ m_{2\_q\_qq}=(F_2(qq)-F_2(q))\bullet \Pr\{in2\}n(n-1)(n(n-1)-2)/8 \\ m_{3\_q\_qq}=(F_3(qq)-F_3(q))\bullet \Pr\{in3\}n(n-1)(n-2)/6 \end{cases} \quad (18)$$

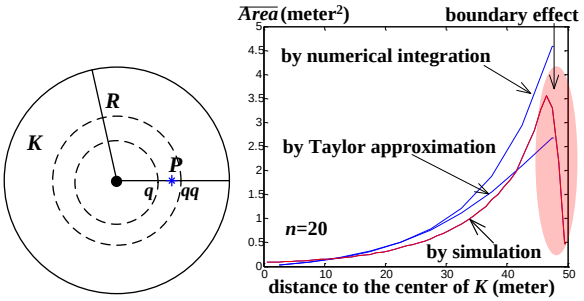

Fig. 8. (a) Annulus q_qq. (b) Average area of polygons in different subregions of K. K is a disk with radius of 50 meters. The number of deployed anchors is n=20. The two solid blue curves are computed by different numerical methods and the red curve is obtained by simulation. The pink shaded region shows the boundary effect of simulation. Without this effect, the simulation curve should continuously go up as the distance increase. See Fig.1b and red circle in Fig.1c for illustration of the boundary effect.

Proof. See Fig.8a, consider an annulus q_qq which respectively bounded by two concentric circles with radius q and qq, we can write the average area of a polygon P whose centroid lies inside annulus q_qq as

$$\overline{Area}_{q\_qq}=\frac{\pi(qq^2-q^2)}{m_{f\_qq}-m_{f\_q}} \quad (19)$$

Where m_{f_qq} and m_{f_q} mean the number of faces (i.e. polygons) lie in circle qq and q, respectively.

By definition 2 and Lemma 2 we can find $\bar{d}_{err}^{local}$. $\blacksquare$

Fig.8b shows that the theoretical evaluation can be used to predict the average area of a polygon in different region of K within reasonable errors as compared to the simulation results, which implies our assumptions and theories about CVD are also reasonable.

4.3 Properties of BCVD

Theorem 8. Given n beacon nodes uniformly distributed in K, the localization error of BCVD is inversely proportional to the square of n.

From theorem 6, we can find point-blank the correctness of theorem 8.

Theorem 9. An on-line implementation of BCVD can be performed by an unknown node within $\Theta(n^2)$ time and $\Theta(n)$ storage, and both are optimal.

Proof. In BCVD an unknown node v updates its AP at most $\Theta(n^2)$ times because the total number of chords is $n(n\text{-}1)/2$ and each update costs $\Theta(1)$ time because the average edge number of an AP is 4. n beacon nodes will incur $\Theta(n)$ storage to be consumed by the $v.SL$.

A CVD scheme has to compute $\Theta(n^2)$ lines in the worst case to form the CVD. Thus BCVD is optimal. $\blacksquare$

To close this section, we would like to point out that even without theorem 2, just by pure mirror image distribution, we still can compute a lower bound for the average area of a polygon in any subregion of K (the proof is omitted). The mirror image distribution is thus considered the most fundamental property of CVD.

5 The Polling Technique

Utilizing only one AP for an unknown-node to locate itself, BCVD actually leaves other $O(n^4)$ APs along with their potential not being fully developed. Can we take advantage of those APs? The answer is yes!

5.1 Principle of the Polling

Proposition 1. Suppose u is a point inside K, there must be at least one AP in CVD contains u.

Definition 3. As shown in Fig.9, two lines, say Line 1 (perpendicular bisector joining A and B) and Line 2 (perpendicular bisector joining $\tilde{A}$ and B), divide the plane into four parts.The *Error Region*(*ER*) is

$$ER=\{H(-sign(\tilde{A}))\cap H(-sign(B))\}\cup\{H(sign(\tilde{A}))\cap H(sign(B))\} \quad (20)$$
$$=H(-\tilde{A},-B)\cup H(\tilde{A},B)$$

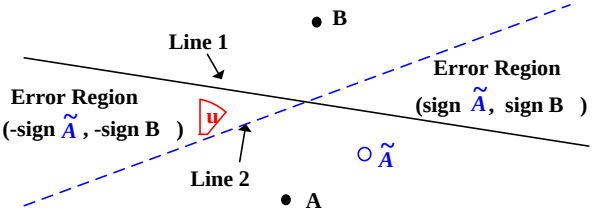

Fig. 9. Illustration for *Error Region* (*ER*). In *ER* A's neighbor node, say u, may detect a conflict when A says its position is $\tilde{A}$. Because in such case $AP_u \cap H(\tilde{A})=\varnothing$, which contradicts to proposition 1. When u lies outside *ER*, such conflict has no chance to be detected.

In Fig.9, let B be a beacon and A a selected unknown node which now wants to position itself. Recall that in BCVD we only take the centroid of AP_A as A's estimate. However, when Polling is enabled, before making the decision, A will select several positions from AP_A as the location propositions and send them to A's neighbors within transmission range. Consider a neighbor u with its AP shown in Fig.9. After comparing the received signal strengths from A and B, u decides it should belong to the $H(sign(A))$. However, if a proposition suggests that A lies at $\tilde{A}$, the perpendicular bisector will then be calculated as Line 2. When u attempts to update its AP, it will result in $AP_u \cap H(sign(\tilde{A}))=\varnothing$ —a conflict is being detected, because proposition 1 states AP_u can not be empty. Thus u declines this proposition and informs A its opinion on $\tilde{A}$.

A's Polling procedure will continue until all the expected feedback messages have been received or a time-

out is triggered. Finally, A will take the centroid of the accepted positions as the estimate.

Due to some reasons (positions, RSS errors, etc.), there has the situation that all A's propositions be declined. In such case, the algorithm will choose the LP (Least Position, i.e. a position with the number of denied-votes is the least) as the estimate. In case more than one position is LP, the algorithm will use the centroid of those LPs as A's final decision (Note: all the accepted positions are LPs — the number of negative votes is zero).

Proposition 2 (principle of Polling). Suppose all nodes uniformly distributed in network region. A proposition receiving smaller number of the negative votes is closer to the real position than that of a proposition receiving larger number of negative votes, on average.

Proposition 2 is based on the following two observations.

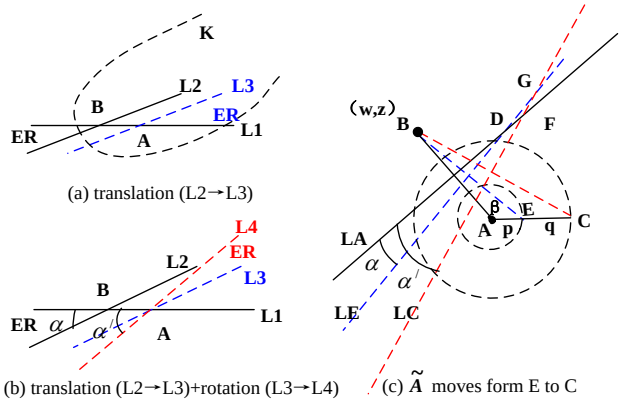

Fig. 10. Illustration for the principle of Polling.

Observation 1. As shown in Fig.10a, when we shift line L2 to L3, which is called the translation, the error region *ER* will change accordingly. Let *ER1* (formed by L2 and L1) denotes the area of $ER \cap K$ before translation, and *ER2* (formed by L3 and L1) the area of $ER \cap K$ after translation, we assert that $\Pr\{ER1 > ER2\} = \Pr\{ER2 > ER1\}$. This is because translation can take place at anywhere in *K*, which equivalents to the procedure that we first form an *ER* and then randomly deploy *K* and compute $K \cap ER$. By symmetry of *ER*, we have the assertion.

In Fig.10b, using the intersection of L3 and L1 as the center, we rotate L3 to L4 after a translation from L2 to L3. Through a similar analysis, we have $\Pr\{ER1 > ER2\} < \Pr\{ER2 > ER1\}$. ■

Observation 2. As shown in Fig.10c, suppose B is a beacon at position (w, z) and A an unknown node which now wants to determine its position. If $\tilde{A}$ (A's proposition) moves along a line passing through B, we shall see the translation of *ER*. Now consider the case that $\tilde{A}$ moving along a ray originated from A. Assume $\tilde{A}$ moves from E to C ($|AE| = p$, $|EC| = q$), the boundary of *ER* will change from LE to LC. Such action can be regarded as a translation ($DF = |q/(2\cos\beta)|$, $\beta = \angle BAC$) plus a rotation ($\angle ABE \to \angle ABC$, or $\alpha \to \alpha'$), which is similar to the process shown in Fig.10b except an extra triangle ΔDFG. The area of ΔDFG ($=pq(p+q)/(8z)$) is finite when $z \neq 0$ (when z=0, we shall see a translation of *ER*). Thus in most situations, we still have *ER2*>*ER1*. So, if $\tilde{A}$ moves from E to C or in other words, moves from a small circle to a larger one (both centered at A), the probability of $\tilde{A}$ suffering more negative votes will increase. ■

5.2 BCVD + Polling

Input: *Anchors*, *UnknownNodes*, *K*, *TransPower*.
Output: position estimates of *UnknownNodes*.

BCVD+POLLING(*Anchors*, *UnknownNodes*, *K*,*TransPower*)
1) **INITIALIZE** (*UnknownNodes*,*K*)
2) **MEASUREMENT**(*Anchors*, *UnknownNodes*, *TransPower*)
3) for each $v \in$ *UnknownNodes*
4) **UPDATE**(*v*)
5) for each $v \in$ *UnknownNodes*
6) **POLLING**(*v*, *Anchors*,*UnknownNodes*,*TransPower*)
7) for each $v \in$ *UnknownNodes* {
8) *v*.LeastPosition ← choose the positions from *v*.PollingPosition whose numbers of negative votes are the least
9) *v*.EstimatedPosition ← centroid(*v*. LeastPosition)
10) }
11) return *UnknownNodes* //with their estimates

POLLING (*v*, *Anchors*, *UnknownNodes*, *TransPower*)
1) *v*.PollingPosition ← uniformly selects several positions from *v*.AP
2) Δ ← randomly selects *t* neighbors of *v* //Δ is a variable; *t* is a predefined positive integer; neighbors including both anchors and unknown nodes
3) Using *TransPower* broadcast *v*.PollingPosition to Δ
4) for each $u \in \Delta$ {
5) for each B $\in$ *Anchors* & B $\neq$ u {
6) for each A $\in$ *v*.PollingPosition {
7) Divides the plane into two half planes by the perpendicular bisector joining A and B. By comparing the measured signal strengths received from *v* and B, u chooses the half plane which *u* believes it should belong to as the *H*(*u*).
8) if *u*.AP $\cap$ *H*(*u*)== $\varnothing$
9) *u* rejects A
10) }
11) }
12) u sends a packet enclosed with its opinion on *v*.PollingPosition to *v*
13) }
14) *v*.PollingPosition ← results of the voting statistics
15) return *v*// with polling results

Theorem 10: Let *t* be the maximum number of the neighbors selected to response to an unknown node's Polling request. Suppose the number of positions selected by any unknown node in its Polling is no more than a constant, the time complexity for performing one Polling request is O(*nt*), and the time complexity of BCVD+Polling is $O(n^2+nt)$.

According to theorem 6, the number of polygons in *K* is $\Theta(n^4)$, thus the maximum effective number of *t* is $O(n^4)$ and a larger value of *t* actually reaps no more fruits. In fact, during Polling, we usually let *t* no more than a constant value or *n*. So BCVD+Polling still can be performed

in O(n^2) time in practice.

5.3 Illustration for BCVD & Polling

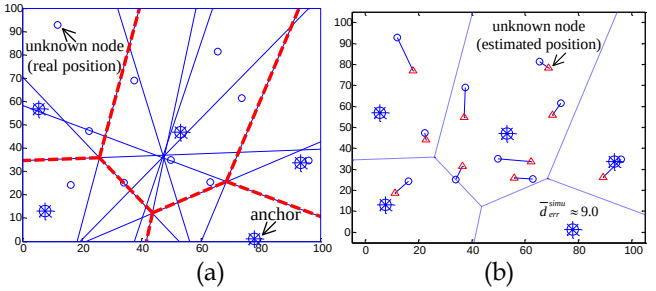

Fig. 11. Illustration for BCVD (RSS errors free). **(a)** The initial nodes distribution and CVD (the UPDATE subroutine is just finished). The red dashed lines show the Voronoi division. **(b)** Overview for the localization error of BCVD. In this picture, unknown nodes locate themselves by taking the centroids of their APs. In signal errors free scenarios, with probability 1, both real and estimated positions of an unknown node are in a common Voronoi cell. In addition, theorem 6 predicts that for this scenario $\bar{d}_{err} \approx 10.4$. Although here K is a square (100×100), the theoretical result is still a reasonable prediction (the average simulation positioning error ≈ 9.0).

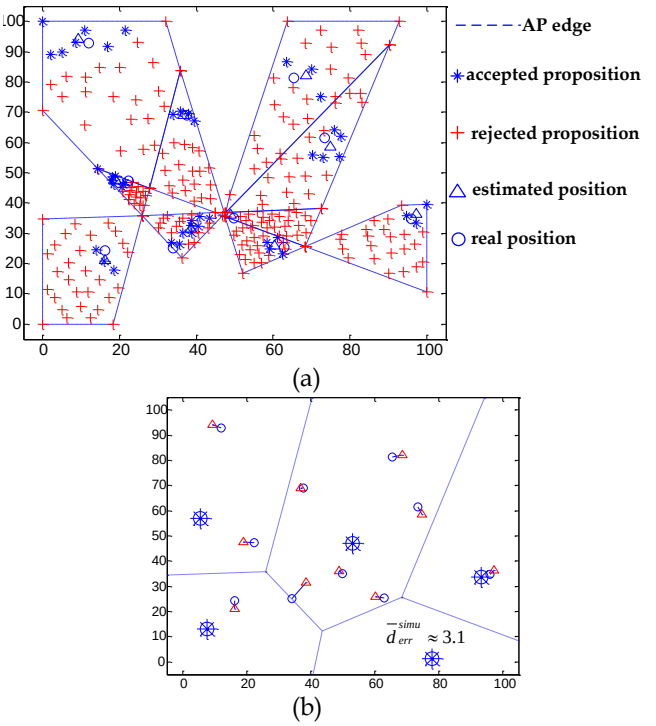

Fig. 12. Illustration for Polling (RSS errors free). **(a)** Polling results for each unknown node; In the AP of the unknown node at (49.8, 35), we can see that even all propositions are declined Polling still can provide us with a good estimation. **(b)** Overview for the localization error of BCVD+Polling. Compared with Fig.11b, Polling reduces more than half of the BCVD's localization error.

6 PERFORMANCE STUDY THROUGH SIMULATIONS

In this section we will: (1) present our strategy for CVD schemes to handle signal errors; (2) show that Polling works in signal errors penetrated scenarios; (3) compare BCVD with some other RSSI based schemes.

6.1 RSS model

We employ a widely used log-norm shadowing model [2, 3] to predict RSSI values:

$$P_R(d) = P_T - P_L(d_0) - 10\eta \log_{10}(d/d_0) + X_\sigma \qquad (21)$$

Where P_R is the received signal power; d is the T-R (Transmitter-Receiver) separation distance; P_T is the transmitter power; $P_L(d_0)$ is the pass loss for a reference distance of d_0; η is the pass loss exponent; X_σ is a Gaussian random variable which denotes the random variation in RSS measurement and $X_\sigma \sim N(0,\sigma^2)$. See table 3.

TABLE 3 [2, 3, 40]
The typical values and ranges for the parameters of simulation

Parameter	Typical value	Typical Range
P_T	4 dBm	-
$P_L(d_0)$	55 (dB), d_0=1m	-
η	4	2-7
σ	4	0-10
n	5,10	5-15
Size of K (a square)	100×100	-

6.2 qADC—a Strategy for Signal Errors Handling

Let $c\sigma$, where c is a positive constant, be a predefined threshold; we modify BCVD and Polling procedure as the following: in step 7 of *UPDATE* subroutine and in step 7 of *POLLING* subroutine, before generating the perpendicular bisector to join two positions, say A and B, the algorithm will make sure that the absolute difference between the two signal strengths (measured from A and B, respectively) is greater than $c\sigma$. Otherwise, the algorithm will silently ignore this beacon pair and turn to the next one. The strategy mentioned above is called qADC (quasi Analog-to-Digital Conversion) due to the similarity between qADC and the traditional ADC. In fact, using qADC, we "safely" translate a real world scenario to a RSS errors near-free scenario at the cost of some reasonable information (or accuracy) loss.

6.3 Performance of BCVD+Polling

See table 4, in most cases, BCVD+Polling performs better than pure BCVD, which implies Polling works even in signal errors presence environments. And the appropriate value of c for typical n under qADC is 2.

The benefit provided by Polling decreases with the growth of σ. However, this is not the Polling's fault. We can hardly imagine other RSSI based schemes can avoid suffering from such baptism.

TABLE 4
Location errors for BCVD and BCVD+Polling under different combinations of n, c, and σ

n	c	σ	BCVD	BCVD+ Polling	n	c	σ	BCVD	BCVD+ Polling
5	0	0	12.3	4.8	10	0	0	4.6	1.3
		2	18.1	13.9			2	11.6	9
		4	22.6	23			4	16.9	15.2
		6	26.6	27			6	23	20.6
		8	29.1	27.2			8	24.2	26.7
		10	36.7	31.5			10	28.8	27.3
	1	2	16.3	10.5		1	2	9	7.6

		4	20.9	16.2		4	14.3	11.6
		6	26.3	21		6	18.4	16.7
		8	29.2	25.7		8	21.7	21.5
		10	31	27.7		10	24.1	22.9
	2	2	18.1	8.7	2	2	9.1	5.4
		4	21.1	13.3		4	13.2	9.5
		6	24.5	19.5		6	15.9	13.7
		8	26.4	22.5		8	19.9	16.8
		10	28.6	25.2		10	20.6	18.4
	3	2	16.3	11	3	2	9.5	6.6
		4	21.9	16.9		4	13.8	10.1
		6	26.5	22		6	16.5	13.1
		8	30	24.7		8	19.5	17.9
		10	30.5	31.9		10	21.9	20.5

6.4 Comparison Between BCVD+Polling and Some Other RSSI Based Localization Schemes

APIT [22]: Utilizing measured RSSI, APIT localizes unknown node by computing the intersection of triangles in which the node resides. However, APIT's constraints on node density, distribution and the transmission radius may not very practical, especially for sparse network. So we modify APIT as: Let 85% of APIT tests be correct.

Proximity: The Proximity scheme [21] localizes unknown node by computing the intersection of communication disks in which the node resides. For simplicity, we set the anchor transmission radius to 0.3×side-length-of-*K*. Directly comparing Proximity with other schemes may not fair for others because in such case Proximity actually does not take any RSS errors into consideration. However, the knowledge gained from Proximity can be the inputs of BCVD+Polling. So we compare Proximity to Proximity+BCVD+Polling.

Multilateration [11,12]: The following estimator is employed in simulation (the interpolating polynomial can be an alternative choice):

$$d = d_0 \times 10^{\frac{P_T - P_L(d_0) - P_R(d)}{10\eta}} \qquad (22)$$

Voronoi scheme: is a virtual localization scheme; it locates unknown node simply by taking the centroid of the Voronoi cell which, based on the measured RSSIs, the unknown node believes itself is reside in.

Main results are as follows: Fig.13 shows that the error performance of BCVD+Polling is better than that of APIT, Proximity and Voronoi. These four schemes are all area-based schemes: they localize nodes by computing some kinds of areas. The accuracy of such schemes mainly depends on two factors: the number and the quality of the utilized areas. In APIT, though the number of anchor-triangles can achieve $O(n^3)$, the quality of those areas are not very satisfactory. Here quality means the coverage and the correctness (1 - the ratio that an unknown node mistakenly believes that it lies in an area which actually not) of the area. A deployment problem of APIT is shown in Fig.14. The major drawbacks of Proximity and Voronoi scheme are the same: the quantity of their utilized areas is only $O(n)$. Therefore, the positioning error decreases only at the speed of $O(n^{1/2})$, while the convergence speed for a CVD based scheme, according to Theorem 8, is $O(n^2)$.

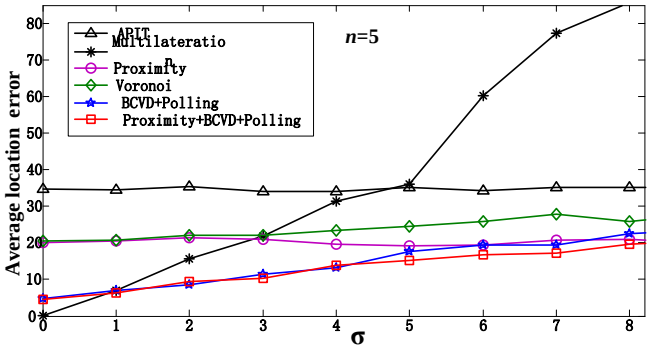

(a) Location errors with varying σ (*n*=5).

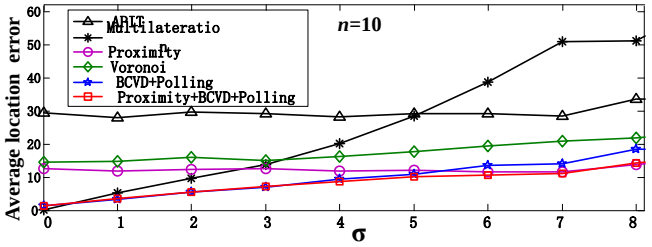

(b) Location errors with varying σ (*n*=10).

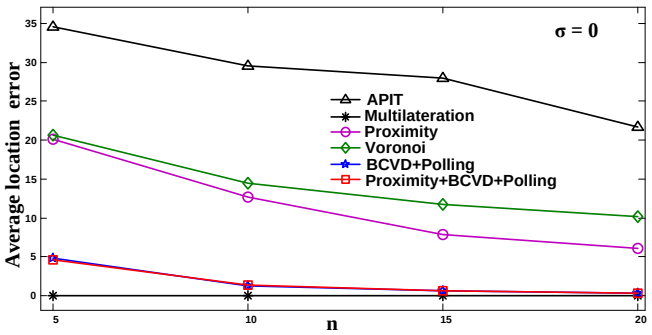

(c) Location errors with varying *n* (σ =0)

Fig. 13 Average location errors of the six schemes: APIT, Multilateration, Proximity, Voronoi, BCVD+Polling and Proximity+BCVD+Polling.

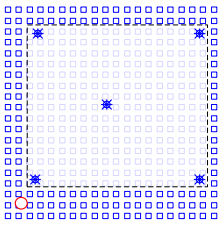

Fig. 14 APIT's coverage problem. No beacon triangle contains the unknown node (red colored point lies at the lower left corner).

Multilateration using MMSE (Minimum Mean Square Estimate) and an ideal estimator (formula (21)) as known priori to provide exact solution (see Fig.13c) for localization when σ=0. In real world, such exact solution does not exist. See Fig.13a and Fig.13b, the real challenge for this scheme is that the localization error grows exponentially with σ [13]. The reason can be inferred from formula (22).

Combined with the Proximity, BCVD+Polling can reduce, though not very significant, some localization errors further. More than the insignificant upgrading of the error performance, the significance of what happened here is that BCVD+Polling can seamlessly take other localization results, sometimes even its own results, as the inputs and refine the previously obtained knowledge.

7 REMARKS

When an unknown node can not hear all beacons directly, it will compute a local CVD (i.e. CVD_{subset}) based on the audible beacons. Those audible beacons are a subset of all beacons, so $CVD_{subset} \subseteq CVD_{overall}$ (the CVD computed on the set of all beacons). In such case, the unknown node may suffer some accuracy loss because its AP might be a collection of polygons in $CVD_{overall}$, and the accuracy performance is thus determined by the number of audible beacons.

For simplicity, we assume K is a disk (including its whole interior region). However, it is not difficult to see that the analysis method can be applied to other scenarios where K is not a disk.

Synchronization, which is highly depended by TOA and TDOA schemes, is not required by BCVD or other CVD based schemes. CVD based schemes, for example BCVD, can be performed in an incremental fashion, which can let algorithm gradually refine the position estimation according to the newly measured signals.

A mobile anchor or moving antenna can provide tremendous number of anchors to a CVD scheme. With the quadratic convergence speed, even using only the cheapest RSSI, a CVD scheme has the potential to quickly achieve the accuracy level we want.

CVD & Polling schemes can be integrated into other localization methods and vice versa to achieve the potential better accuracy performance. Regarding the original scheme as an optimization problem, to locate an unknown node u, for each edge of AP_u we simply add a linear inequality constraint (based on the received signal strengths and the coordinates of the corresponding anchor pairs) to the original constraint set; for Polling, we first compute a convex hull or a bounding box of the least positions, and then for each boundary edge we add a constraint to the original constraint set. In this way, other schemes can take full advantage of CVD and Polling.

CVD based schemes can be applied in both indoor and outdoor environments.

CVD based algorithms do not need to directly translate a signal to the Euclidean distance. It does not matter what kind of communication model be employed. GCM (Gauss Channel Model), Rayleigh fading channel model or other physical models are all the same from CVD's perspective. What a CVD scheme really cares about is the relative difference between measurements. Any measurement changing roughly monotonically with the distance can be applied by CVD schemes. Such measurements are common in natural world. Other than RSSI, we can use TOA, hops of traveling packets, strength of acoustic wave, concentration of chemicals, gravity of objects, etc. for localization. Actually, we can hardly imagine what kind of communication signal has no properties changing roughly monotonically with the distance.

8 CONCLUSION

CVD scheme together with Polling and qADC can provide a simple, robust and powerful solution to the wireless network localization.

ACKNOWLEDGMENTS

This work was supported in part by the Fundamental Research Funds for the Central Universities under grant No. GK201002034, GK200902018, GK201401002, Shaanxi Normal University, China; Ph.D. Programs Foundation of Ministry of Education of China under grant No. 20110202120002; the National Natural Science Foundation of China under grant No. 61100239, 61373083, 61173094, 61173190, 61402273, 61402274, 11101012159, 11502133; The Program of Shaanxi Science and Technology Innovati on Team under grant no. 2014KTC-18;

The research of Li is partially supported by NSF ECCS-1247944, NSF ECCS-1343306, NSF CMMI 1436786.

The authors thank Xiaolin Hu for his comments on the draft.

REFERENCES

[1] Lyudmila Mihaylova, Donka Angelova, David R. Bull and Nishan Canagarajah, "Localization of Mobile Nodes in Wireless Networks with Correlated in Time Measurement Noise", IEEE Transaction on Mobile Computing, vol. 10, no. 1, pp.44-53, Jan. 2011.

[2] P. Bahl and V. N. Padmanabhan, "RADAR: An In-Building RF-Based User Location and Tracking System," In Proceedings of the IEEE INFOCOM '00, March 2000, pp. 775-784 vol. 2.

[3] T. S. Rappaport, Wireless Communications Principles and Practice. Upper Saddle River, NJ: Prentice Hall, second ed., 2002.

[4] G. Zhou, T. He, S. Krishnamurthy, and J. A. Stankovic, "Models and solutions for radio irregularity in wireless sensor networks," ACM /Transactions on Sensor Networks, vol. 2, no. 2, pp. 221–262, May 2006.

[5] B. H. Wellenhoff, H. Lichtenegger and J. Collins, Global Positions System: Theory and Practice, Fourth Edition, Springer Verlag, 1997.

[6] Wenchao Huang, Yan Xiong, Xiang-Yang Li, Hao Lin, XuFei Mao, Panlong Yang, Yunhao Liu, Xinfu Wang, "Swadloon: Direction Finding and Indoor Localization Using Acoustic Signal by Shaking Smartphones," IEEE Transaction on Mobile Computing, November, 2014.

[7] JiZhong Zhao, Wei Xi, Yuan He, YunHao Liu, Xiang-Yang Li, LuFeng Mo, and Zheng Yang, "Localization of Wireless Sensor Networks in the Wild: Pursuit of Ranging Quality," IEEE/ACM Transactions on Networking, vol. 21, no. 1, pp. 311–323, Feb. 2013.

[8] N. B. Priyantha, A. Chakraborty and H. Balakrishnan, "The Cricket Location-Support System," In Proceedings of MOBICOM '00, New York, August 2000, pp. 32-43.

[9] D. Niculescu and B. Nath, "Ad hoc positioning system (APS) using AOA," in Proceedings of IEEE INFOCOM 2003, 30 March-3 April 2003, pp. 1734-1743 vol. 3.

[10] R. Want, A. Hopper, V. Falcao, J. Gibbons, "The active badge location system," ACM Trans. on Information Systems, vol. 10, no. 1, pp. 91-102, Jan. 1992.

[11] A. Savvides, C. C. Han and M. B. Srivastava, "Dynamic Fine- Grained Localization in Ad-Hoc Networks of Sensors," In Proceedings of MOBICOM '01, Rome, Italy, July 2001, pp. 166-179.

[12] A. Savvides, H. Park and M. Srivastava, "The Bits and Flops of the N-Hop Multilateration Primitive for Node Localization Problems," In First ACM International Workshop on Wireless Sensor Networks and Application, Atlanta, GA, September 2002, pp. 112-121.

[13] Sree Divya Chitte, Soura Dasgupta and Zhi Ding, "Distance Estimation from Received Signal Strength under Log-Normal Shadowing: Bias

and Variance". IEEE Signal Processing Letters, vol. 16, no. 3, pp. 216-218, Mar. 2009.

[14] Cheng Bo, Xiang-Yang Li, Taeho Jung, XuFei Mao, Yue Tao, Lan Yao., "SmartLoc: push the limit of the inertial sensor based metropolitan localization using smartphone," in Proceeding of MobiCom '13, September 30–October 4, 2013, Miami, FL, USA, pp. 195-198.

[15] Ismail G¨uvenc and Chia-Chin Chong, "A Survey on TOA Based Wireless Localization and NLOS Mitigation Techniques," IEEE Communications Surveys & Tutorials, vol. 11, no. 3, pp. 107-124, Aug. 2009.

[16] Zheng Yang, YunHao Liu, Xiang-Yang Li, "Beyond Trilateration: On the Localizability of Wireless Ad-hoc Networks," IEEE/ACM Transactions on Networking, vol. 18, no. 6, pp. 1806–1814, Dec. 2010.

[17] D. Niculescu and B. Nath, "Dv based positioning in ad hoc networks," Journal of Telecommunication Systems, vol. 22, no. 1, pp. 267–280, January 2003.

[18] Lei Yang, Yekui Chen, Xiang-Yang Li, Chaowei Xiao, Mo Li, Yunhao Liu, "Tagoram: Real-Time Tracking of Mobile RFID Tags to High Precision Using COTS Devices," in Proceeding of MobiCom '14, September 07-11, 2014, Maui, Hawaii, USA, pp. 237-248.

[19] Lan Zhang, Kebin Liu, Yonghang Jiang, Xiang-Yang Li, YunHao Liu, Panlong Yang, "Montage: Combine Frames with Movement Continuity for Realtime Multi-User Tracking," in Proc. IEEE Conf. Comput. Commun., 2014, pp. 799–807.

[20] L. Doherty, K. S. J. Pister, L. El Ghaoui, "Convex position estimation in wireless sensor networks," In: Proc. of the IEEE INFOCOM 2001, 2001, pp. 1655-1663 vol. 3.

[21] N. Bulusu, J. Heidemann, and D. Estrin, "GPS-less low cost outdoor localization for very small devices," IEEE Personal Communications Magazine, vol. 7, no. 5, pp. 28–34, October 2000.

[22] T. He, C. Huang, B. Blum, J. Stankovic, and T. Abdelzaher, "Range-free localization and its impact on large scale sensor networks," ACM Transactions on Embedded Computing Systems, vol. 4, no. 4, pp. 877-906, Nov. 2005.

[23] Y. Shang, W. Ruml, Y. Zhang, and M. Fromherz, "Localization from mere connectivity," in Proceedings of the 4th ACM international Symposium on Mobile ad hoc networking & computing, 2003, pp. 201–212.

[24] James Aspnes, Tolga Eren, David K. Goldenberg, A. Stephen Morse, Walter Whiteley, Yang Richard Yang, Brian D.O. Anderson, Peter N. Belhumeur, "A Theory of Network Localization," IEEE Transactions on Mobile Computing, vol. 5, no. 12, pp. 1663-1678, Dec. 2006.

[25] N. Ruana and D.Y. Gao, "Global Optimal Solutions to General Sensor Network Localization Problem," Performance Evaluation (ELSEVIER), vol. 75–76, pp. 1–16, May–June 2014.

[26] T. Liu, L. Yang, Q. Lin, Y. Guo, and Y. Liu, "Anchor-free backscatter positioning for rfid tagswith high accuracy," in Proc. of IEEE INFOCOM 2014, April 27 2014-May 2, 2014, pp. 379-387.

[27] M. Nicoli, C. Morelli, V. Rampa, "A Jump Markov Particle Filter for Localization of Moving Terminals in Multipath Indoor Scenarios," Signal Processing, IEEE Transactions on, vol. 56, no. 8, Part 1, pp. 3801 – 3809, Aug. 2008.

[28] S. H. Fang, T. N. Lin, "Indoor Location System Based on Discriminant-Adaptive Neural Network in IEEE 802.11 Environments," Neural Networks, IEEE Transactions on, vol. 19, no. 11, pp. 1973 – 1978, Nov. 2008.

[29] J. Kosecka, F. Li, "Vision based topological Markov localization," in Proceedings of 2004 IEEE International Conference on Robotics and Automation, April 26-May 1, 2004, pp. 1481–1486 vol. 2.

[30] F. P. Preparata, M. I. Shamos, Computational Geometry: An Introduction, Springer, Berlin, 1985.

[31] J. Hightower, G. Boriello and R. Want, "SpotON: An indoor 3D Location Sensing Technology Based on RF Signal Strength," University of Washington, CSE Report #2000-02-02, February 2000, http://ahvaz.ist.unomaha.edu/azad/temp/sal/00-hightower-localization-indoor-3d-rssi-spoton-techrep.pdf.

[32] Gerhard P. Hancke and Ben Allen, "Ultrawideband as an Industrial Wireless Solution," IEEE Pervasive Computing, vol. 5, no. 4, pp. 78-85, October-December 2006.

[33] K. Chintalapudi, A. Padmanabha Iyer, and V. N. Padmanabhan, "Indoor localization without the pain," In Proceeding of ACM MobiCom '10, 2010, pp. 173-184.

[34] A. Rai, K. K. Chintalapudi, V. N. Padmanabhan, and R. Sen, "Zee: zero-effort crowdsourcing for indoor localization," In Proceeding of ACM Mobicom '12, 2012, pp. 293-304.

[35] Moe Z. Win, Robert A. Scholtz, "Impulse Radio: How It Works," IEEE Communications Letters, vol. 2, no. 2, pp. 36-38, Jan. 1998.

[36] Nayef A. Alsindi, Bardia Alavi, Kaveh Pahlavan, "Measurement and Modeling of Ultrawideband TOA-Based Ranging in Indoor Multipath Environments," IEEE Transactions on Vehicular Technology, vol. 58, no. 3, pp. 1046-1058, May 2009.

[37] B. T. Fang, "BSimple solutions for hyperbolic and related position fixes," IEEE Trans. on Aerosp. Electron. Syst., vol. 26, no. 5, pp. 748–753, Sep. 1990.

[38] Yuan Shen, Wenhan Dai, Moe Z. Win, "Power Optimization for Network Localization," IEEE/ACM Transactions on Networking, vol. 22, no. 4, pp. 1337-1350, Sep. 2013.

[39] S. Nirjon and J. Stankovic, "Kinsight: Localizing and tracking household objects using depth-camera sensors," in 2012 IEEE 8th International Distributed Computing in Sensor Systems (DCOSS), May 2012, pp. 67-74

[40] Kiran Yedavalli and Bhaskar Krishnamachari, "Sequence-Based Localization in Wireless Sensor Networks," IEEE transactions on Mobile Computing, vol. 7, no. 1, pp. 81-94, Jan. 2008.

[41] Y. Jie, Y. Qiang, and N. Lionel, "Learning Adaptive Temporal Radio Maps for Signal-Strength-Based Location Estimation," IEEE Trans. Mobile Computing, vol. 7, no. 7, pp. 869-883, July 2008.

[42] Jue Wang, Fadel Adib, Ross Knepper, Dina Katabi, Daniela Rus, "RF-Compass: Robot Object Manipulation Using RFIDs," in Proceedings of ACM MobiCom '13, September 30–October 4, Miami, FL, USA, pp. 3-14.

[43] J. Wang and D. Katabi, "Dude, Where's my card?: RFID Positioning That Works with Multipath and Non-Line of Sight," in Proceedings of ACM SIGCOMM '13, Oct. 2013, pp. 51-62.

[44] Kaishun Wu, Jiang Xiao, Youwen Yi, Min Gao, Lionel M. Ni, "Fila: Fine-grained indoor localization," in Proceedings of INFOCOM 2012, pp. 2210–2218.

[45] Jiang Xiao, Youwen Yi, Lu Wang, Haochao Li, Zimu Zhou, Kaishun Wu and Lionel M. Ni, "NomLoc: Calibration-free Indoor Localization With Nomadic Access Points," in Proceedings of IEEE 34th International Conference on Distributed Computing Systems, June 30 2014-July 3 2014, pp. 587-596.

Dr. Gang Lu received the PhD degree in computer science from University of Electronic Science and Technology of China in 2009. He is an associate professor in School of Computer Science, Shaanxi Normal University, Xian, Shaanxi Province, China. He was a visiting researcher with Illinois Institute of Technology from 2014 to 2015. His research interests are in computational geometry, graph theory, artificial intelligence, software

engineering and their applications in wireless networks. He is a member of the ACM and a member of the IEEE CS.

Mingtian Zhou is a professor of computer science in School of Computer Sciences and Engineering, University of Electronic Science and Technology of China, Chengdu, Sichuan Province, China. His research interests include the network computing, mobile ad hoc networks and information security. He is a senior member of the IEEE.

Dr. Xiaoming Wang received the PhD degree in computer theory and software engineering from Northwest University, China, in 2005. He is a professor in School of Computer Science, Shaanxi Normal University. From 2007 to 2008, he was a research professor at Georgia State University. His research interests include network security, access control, pervasive computing and wireless sensor networks.

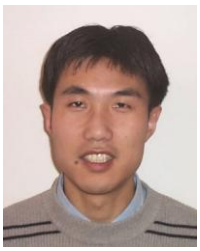

Dr. Xiang-Yang Li (M'99-SM'08-F'15) is a professor of Computer Science at the Illinois Institute of Technology, a visiting professor at University of Science and Technology of China, and EMC Visiting Chair Professor at Department of Computer Science, Tsinghua University. He is a recipient of China NSF Outstanding Overseas Young Researcher (B) in 2008. He received MS (2000) and PhD (2001) degree at Computer Science Department from University of Illinois at Urbana-Champaign, B.Eng. at Computer Science and Bachelor degree at Business Management from Tsinghua University, P.R. China in 1995. His research interests include wireless networks, big data privacy and security, cyber physical systems, and social networks. He and his students won four best paper awards (IEEE IPCCC 2014, ACM MobiCom 2014, COCOON 2001, IEEE HICSS 2001), one best demo award (ACM MobiCom 2012) and was selected as best paper candidates three-times (BigCom 2015, ACM MobiCom 2008, ACM MobiCom 2005). He serves as an editor of several journals, including"IEEE TMC", and was an editor of "IEEE TPDS". He is an IEEE Fellow and an ACM Distinguished Scientist.

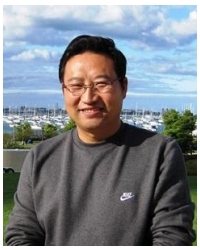

Dr. Xiaojun Wu is a professor of computer science in School of Computer Science, Shaanxi Normal University, Xian, Shaanxi Province, China. His research interests focus on chaotic signal analysis and wireless ad hoc networks.

Dr. Yumei Zhang is an associate professor in School of Computer Science, Shaanxi Normal University, Xian, Shaanxi Province, China. Her research interests including the speech signal processing, chaotic signal analysis and the city traffic flow management.